16th World Conference on Earthquake, 16WCEE 2017
Santiago Chile, January 9th to 13th 2017
Paper N° 705 (Abstract ID)
Registration Code: S- R1463193737

Effect of the principal stress direction on undrained cyclic behaviour of saturated silt using a hollow cylinder apparatus

Zhou Zhenglong(1), Chen Guoxing(2), Xu Lingyu(3), Zhao Kai (4)

(1) *PhD student, Institute of Geotechnical Engineering, Nanjing Tech University, Nanjing, China, zhouzhen.glong@163.com*
(2) *Professor, Institute of Geotechnical Engineering, Nanjing Tech University, Nanjing, China, gxc6307@163.com*
(3) *Lecturer, Institute of Geotechnical Engineering, Nanjing Tech University, Nanjing, China, xulingyu2008@126.com*
(4) *Lecturer, Institute of Geotechnical Engineering, Nanjing Tech University, Nanjing, China, zhaokaiseu@aliyun.com*

Abstract

The impact of fabric anisotropy on the behaviour of soil has been paid great attention; however, the effects of the principal stress direction on the cyclic undrained response of saturated silt are not fully understood. An experimental study aimed at providing insights into the effect of principal stress direction on the cyclic behaviour of saturated silt with a relative density of 50% under isotropic consolidation condition is presented. A series of cyclic shear tests were conducted by GDS hollow cylinder torsional apparatus that can apply four dynamic loads, namely inner pressure, outer pressure, axial load and torque. Specimens at identical initial states were subjected to 90° jump rotation of principal stresses from different principal stress direction angle $\alpha_{\sigma 0}$ at the initial time of cyclic loading with a constant intermediate principal stress coefficient. This investigation was placed on the influence of $\alpha_{\sigma 0}$ on the pore pressure response, deformation characteristics and cyclic shear strength. The results show that the principal stress direction has a considerable influence on cyclic shear strength of saturated silt. It decreases significantly as the $\alpha_{\sigma 0}$ increased to approximately 45°, and then increases with the $\alpha_{\sigma 0}$ increased to 90°. This observation is considered to be directly related to the soil fabric anisotropy.

Keywords: silt, principal stress direction, excess pore pressure, deviatoric strain, Cyclic shear strength

1. Introduction

Natural soil deposits is known for inherently anisotropic because of the mode of deposition and the particle orientation in the deposition process[1]. This inherent anisotropy highlights the fact that the resistance characteristics are influenced by the change in the magnitudes and directions of the principal stresses acting on soil deposits. In recent years, the anisotropy behaviour of granular soils in undrained conditions has been observed by many researchers[2-6]. These studies illustrated the direction of loading has significant influence on the strength and deformation behaviour of granular soils.

Most of the investigations on the effect of the principal stress direction have focused on the undrained monotonic shear behaviour. However, there have been very limited attempts to study the principal stress direction on cyclic behaviour of granular soils due to the limitation of the laboratory testing devices. Triaxial and simple shear devices have limited control of principal stress direction and its rotation and can only follow specific loading paths. Using a hollow cylinder apparatus, Sato and Yoshida [7] investigated the effect of principal stress direction on the response of a dense sand. In their tests the major principal stress was 90° jump rotated from different initial loading direction. Meanwhile, the mean principal stress p and intermediate principal stress coefficient b were held constant during loading. The results showed that the weakest response at a minimum resistance at failure for the principal stress direction angle at the initial time of cyclic loading up to 45°. More recently Sivathayalan et al. [8] conducted a systematic study to assess the role of principal stress rotation on the cyclic resistance of sands at an intermediate principal stress coefficient $b = 0$ and noted that cyclic resistance decreased significantly with the maximum orientation of the major principal stress increased to approximately 45°–60° and then increased with further rotation. Clearly, most investigations have focused on the effect of principal stress direction on cyclic resistance of sands. However, Silty materials are also known to liquefy, which are somewhat more complicated than sands. Therefore, there is a need to improve understanding the effect of principal stress direction on silt.

This paper presents an experimental study on the influence of the principal stress direction on cyclic behaviour of a saturated silt, including the development of excess pore pressure and deformation and cyclic shear strength.

2. Test procedures

2.1 Experiment equipment and principles

The test equipment adopted in this study is the hollow cylinder apparatus (HCA) manufactured by GDS Instruments (Fig. 1). Four stress components including the vertical (axial) load W, torque M_T, outer cell pressure p_o, and inner cell pressure p_i can be controlled independently by the equipment (Fig. 2a). Fig. 2b shows the corresponding axial stress σ_z, the radial stress σ_r, tangential stress σ_θ and shear stress $\tau_{z\theta}$ acting on a element in the wall of a hollow cylinder sample. By controlling these stresses, the major principal stresses σ_1, intermediate principal stresses σ_2 and minor principal stresses σ_3 in Fig. 2c can be independently controlled. Considering the hollow cylinder as an element, the stress and strain components which are calculated based mainly on the studies of Hight et al. [9] and Miura et al. [10], are shown in Table 1.

Fig. 1 – GDS Hollow Cylinder Apparatus

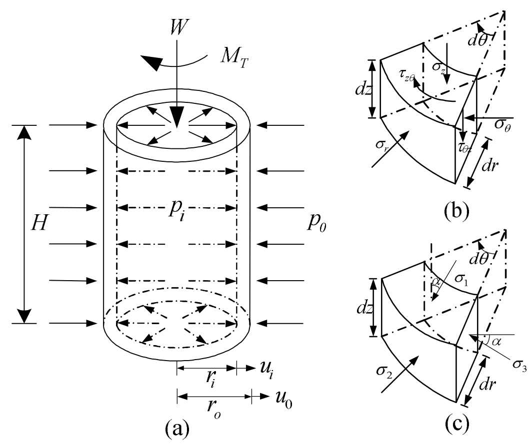

Fig. 2 – Hollow Cylinder specimen

The stress state of the specimen was expressed using the mean principal stress p, deviatoric stress q, intermediate principal stress coefficient b and the angle of the maximum principal stress from the vertical axis α. these Parameters are calculated by the following equations:

$$p == \frac{(\sigma_1 + \sigma_2 + \sigma_3)}{3} \tag{1}$$

$$q = \sigma_1 - \sigma_3 \tag{2}$$

$$b = \frac{\sigma_2 - \sigma_3}{\sigma_1 - \sigma_3} \tag{3}$$

$$\alpha = \frac{1}{2}\arctan\frac{2\tau_{z\theta}}{\sigma_z - \sigma_\theta} \tag{4}$$

The deviatoric strain is used to represent the deformation as given in the following equations:

$$\gamma_q = \varepsilon_1 - \varepsilon_3 \tag{5}$$

Table 1 – Equations for data interpretation

	Stress	Strain
Vertical	$\sigma_z = \dfrac{W}{\pi(r_o^2 - r_i^2)} + \dfrac{p_o r_o^2 - p_i r_i^2}{(r_o^2 - r_i^2)}$	$\varepsilon_z = \dfrac{z}{H}$
Radial	$\sigma_r = \dfrac{p_o r_o + p_i r_i}{r_o + r_i}$	$\varepsilon_r = -\dfrac{(u_o - u_i)}{(r_o - r_i)}$
Circumferential	$\sigma_\theta = \dfrac{p_o r_o - p_i r_i}{r_o - r_i}$	$\varepsilon_\theta = -\dfrac{(u_o + u_i)}{(r_o + r_i)}$
Shear	$\tau_{z\theta} = \dfrac{3M_T}{2\pi(r_o^3 - r_i^3)}$	$\gamma_{z\theta} = \dfrac{2\theta(r_o^3 - r_i^3)}{3H\left(r_o^2 - r_i^2\right)}$
Major principal	$\sigma_1 = \dfrac{\sigma_z + \sigma_\theta}{2} + \sqrt{\left(\dfrac{\sigma_z - \sigma_\theta}{2}\right)^2 + (\tau_{z\theta})^2}$	$\varepsilon_1 = \dfrac{\varepsilon_z + \varepsilon_\theta}{2} + \sqrt{\left(\dfrac{\varepsilon_z - \varepsilon_\theta}{2}\right)^2 + (\gamma_{z\theta})^2}$
Intermediate principal	$\sigma_2 = \sigma_r$	$\varepsilon_2 = \varepsilon_r$
Minor principal	$\sigma_3 = \dfrac{\sigma_z + \sigma_\theta}{2} - \sqrt{\left(\dfrac{\sigma_z - \sigma_\theta}{2}\right)^2 + (\tau_{z\theta})^2}$	$\varepsilon_3 = \dfrac{\varepsilon_z + \varepsilon_\theta}{2} - \sqrt{\left(\dfrac{\varepsilon_z - \varepsilon_\theta}{2}\right)^2 + (\gamma_{z\theta})^2}$

Notes: r_o, outer radius; r_i, inner radius; H, height of specimen; z, axial deformation; u_o and u_i, radial deformations of the outer and inner walls calculated from the change of inner and outer volumes, respectively, assuming that the specimen deforms as a right cylinder; θ, torsional deformation.

2.2 Sample preparation

The soil used in the tests was supplied in powdered form from Nantong, China The particle size distribution and optical microscope image of the silt are presented in Fig. 3. The material consisted of 57.7% silt, 1.3% clay, and 41.0% fine sand size particles. The physical properties of the silt used in the tests were given in Table 2. The hollow cylinder specimen has initial dimensions of 60 mm inner diameter, 100 mm outer diameter and 200 mm in height. The dry deposition method was used for the sample preparation. The total weight of the oven-dried specimen was calculated for a specified unit weight. The specimens were prepared in eight equal-mass layers in the dry state, and each layer of silt of the specimen was poured into the hollow space between two molds with a spoon and a funnel. Maintenance of a zero falling head was attempted, and the outer mold was tapped gently using a rubber mallet to adjust the specified relative density of approximately 50% of the sample, layer by layer. After tamping one layer, the layer interface of the specimen was sufficiently rough to ensure that the two layers could be integrated. After filling with dry silt, the specimens were saturated by circulating both CO_2 and de-aired water, combined with a back pressure of 400 kPa to ensure Skempton's B-value parameter with a value higher than 0.97. Both outer and inner cell pressure were then increased to make the specimens isotropically consolidated to an effective stress state up to 100 kPa.

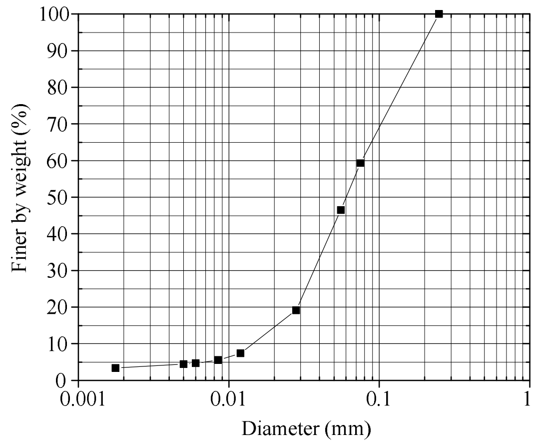

Fig. 3 – Grain size distribution curve of silt

Table 2 Physical properties of the silt used in the tests

Plastic Index PI	**Specific gravity** G_s	**Maximum void ratio** e_{max}	**Minimum void ratio** e_{min}
3	2.70	1.14	0.62

2.3 Test program

After being consolidated, stress-controlled undrained tests were carried out. It should be noted that both the mean principal stress (p = 100 kPa) and the intermediate principal stress coefficient (b = 0) were maintained constant during all tests. It is stated by Tatsuoka et al. [11] that the effect of the loading frequency between 0.05 Hz and 1.0 Hz is very little. A sinusoidal, constant stress amplitude cyclic deviator stress was applied at a frequency of 0.1 Hz in the undrained condition to guarantee precise control of the shape of the stress path. The stress paths of the undrained cyclic shear tests with fixed and reversed orientation of principal stress axes performed in deviatoric stress space are schematically explained in Fig. 4(a). The imposed paths correspond to the lines of different slope in deviatoric stress space. All tests were conducted with 90° jump rotation of principal stresses where the slope of a line path was dependent on the orientation of the major principal stress relative to the vertical direction of the sample at the initial time of sequence of cyclic loading. The principal stress direction angle at the initial time of cyclic loading was defined as $\alpha_{\sigma 0}$ in Fig. 4(b), which was varied from 0° to 90°. In order to specify the three dimensional stress condition, it is necessary to introduce the shear stress τ [12,13] which is a function of $(\sigma_1-\sigma_3)/2$ as shown in Fig. 4(b).In all tests the orientation of the major principal stress α was maintained at $\alpha_{\sigma 0}$ for half the cycle and then switched to $90° - \alpha_{\sigma 0}$ for the other half (Fig. 4(c)), while the shear stress was applied as sinusoidal cycle (Fig. 4(d)).

Cyclic stress ratio CSR in hollow cylinder tests is normally defined by normalizing the maximum cyclic shear stress τ_{cy} by the effective mean confining stress $p_0^{'}$ .Because all specimens were hydrostatically consolidated, this definition is identical to the commonly used CSR = τ_{cy} / $p_0^{'}$ in cyclic torsional tests. The initial conditions for the specimen are summarized in Table 3.

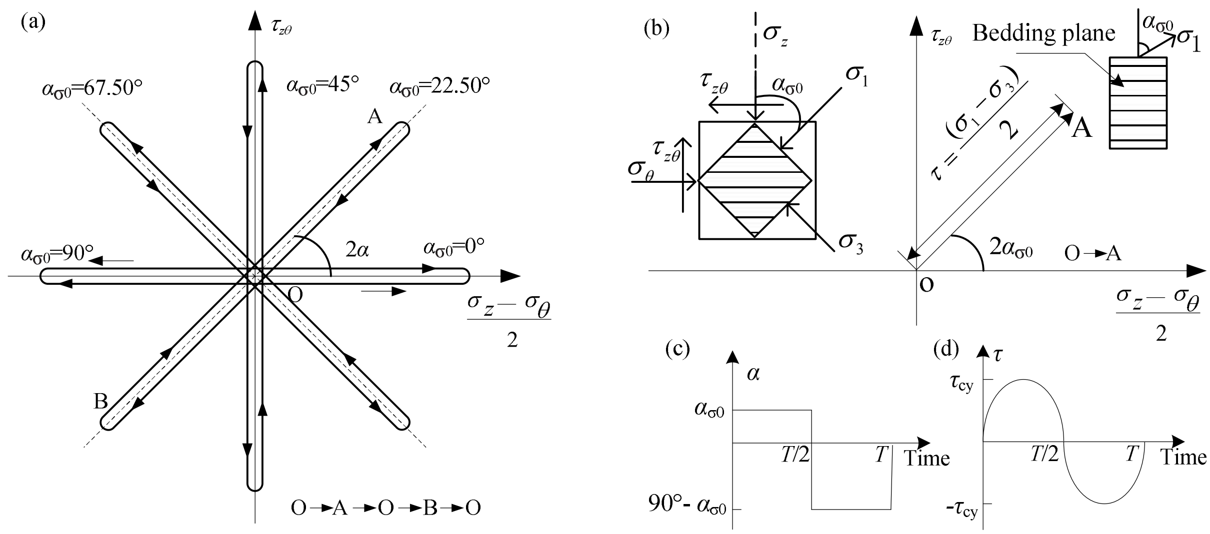

Fig. 4 – Stress path for cyclic loading

Table 3 undrained cyclic torsional tests

Case ID	Effective mean confining stress p_0' (kPa)	The intermediate principal stress coefficient b	Initial loading principal stress direction $\alpha_{\sigma0}$ (°)	Cyclic stress ratio CSR= $\tau_{cy} / 2\, p_0'$
C1	100	0.5	0	0.10
C2	100	0.5	0	0.15
C3	100	0.5	0	0.20
C4	100	0.5	22.5	0.10
C5	100	0.5	22.5	0.15
C6	100	0.5	22.5	0.20
C7	100	0.5	45	0.10
C8	100	0.5	45	0.15
C9	100	0.5	45	0.20
C10	100	0.5	67.5	0.10
C11	100	0.5	67.5	0.15
C12	100	0.5	67.5	0.20
C13	100	0.5	90	0.10
C14	100	0.5	90	0.15
C15	100	0.5	90	0.20

3. Test results and analysis

Fig. 5 shows the typical variations of mean principal stress, deviatoric stress, intermediate principal stress coefficient, principal stress direction, deviatoric strain and excess pore pressure with the number of cycles for $\alpha_{\sigma 0}$=22.5° with CSR = 0.15. It can be observed that the magnitude of the mean principal stress and intermediate principal stress coefficient is maintained constant but the direction of the major principal stress and the deviatoric stress are cyclic varied. Meanwhile, with loading proceeded, excess pore water pressure is gradually built up until it reaches the initial effective confining stress and then failure is characterized by initial liquefaction with zero effective mean principal stress. The initial liquefaction occurs with a sudden development of excess pore pressure near the final stages of cyclic loading preceded by a sudden increase in deviatoric strain.

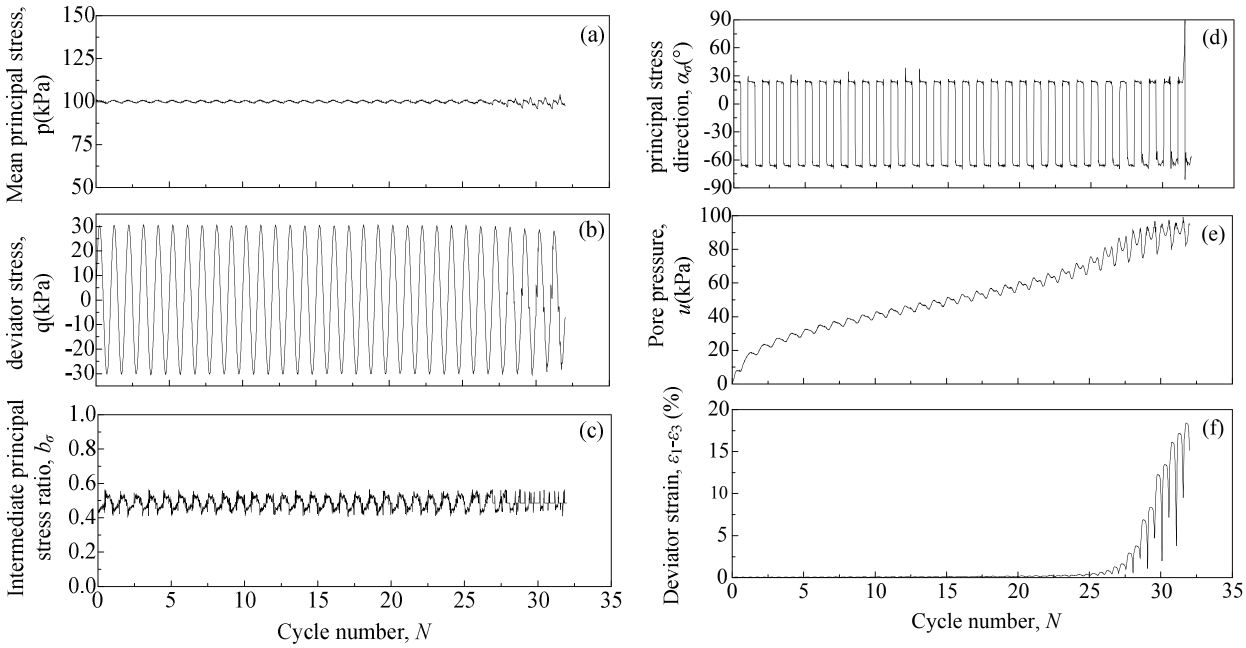

Fig. 5 – The test results for sample C5 ($\alpha_{\sigma 0}$=22.5°, CSR = 0.15).

3.1 Effect of principal stress direction on the development of excess pore pressure

Excess pore pressures are often quantified in terms of pore pressure ratio. The pore pressure ratio r_u is defined as the ratio of the excess pore pressure u and the mean confining stress $p_0^{'}$ acting on the soil (i.e., $r_u = u/p_0^{'}$). Fig. 7 shows a relationship between the number of cycles N and the excess pore pressure ratio r_u for each number of cycles with $\alpha_{\sigma 0}$ = 0°, 22.5°, 45°, 67.5° and 90.0° at CSR levels of 0.10, 0.15 and 0.20. It is clear that the development of excess pore pressure was dependent on the principal stress direction and the cyclic stress ratio. The rate of pore pressure generation under the condition $\alpha_{\sigma 0}$ = 45° was much faster than that under the other conditions, regardless of the cyclic stress ratio. Comparison between Figs 8(a), 8(b) and (c) suggests that the effect due to the change of the deviatoric stress magnitude was also considerable: the larger the CSR applied, the faster the pore pressure rise. It is interesting to note that the difference in pore pressure response with $\alpha_{\sigma 0}$ = 0°, 22.5°, 45°,67.5° and 90° tends to become smaller at the higher level of CSR.

In Fig. 7 the excess pore water pressure accumulation during cyclic loading has been plotted against cyclic ratio N/N_L, where N/N_L is the ratio of the current number of cycles N and the number of cycles required to develop a pore pressure ratio r_u =1. This method of plotting excess pore pressure development as a function of the number of loading cycles ratio was used in some studies [14,15]. It can be observed that the r_u versus N/N_L curves display hardly any change with the increase of $\alpha_{\sigma 0}$, but the r_u versus N/N_L curves dependent on CSR. The double normalized pore pressure development can be roughly categorized into three types for CSR levels of 0.10, 0.15 and 0.20. For the first type at CSR = 0.10, the r_u versus N/N_L curve can be divided into three stages marked by two inflection points. In the first and third stages, pore pressure is generated rapidly, whereas it increases only steadily in the second stage accompanied. The second type for CSR= 0.15 is similar to the first except for the inflection points far from the liquefaction cycles. For the third type at CSR= 0.15, the curve is characterized by the double normalized pore pressure generation in a hyperbolic way with no obvious inflection point.

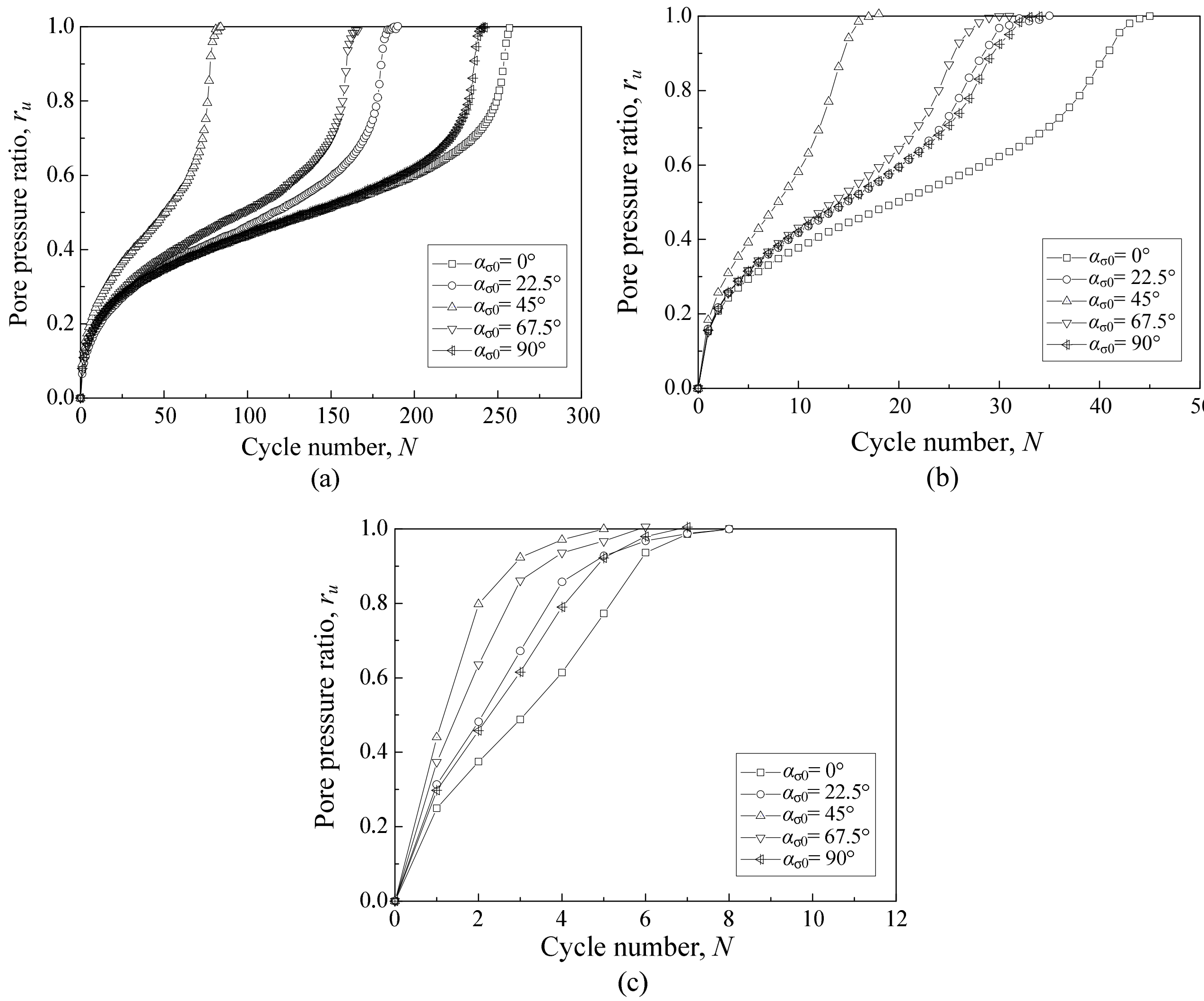

Fig.6 – The relationship between initial loading direction $\alpha_{\sigma 0}$, pore pressure ratio r_u, and the number of cycles N for the different cyclic stress ratio CSR: (a) CSR = 0.10; (b) CSR = 0.15; (c) CSR = 0.20

3.2 Effect of principal stress direction on the development of deviatoric strain

Fig. 8 shows a relationship between the number of cycles and deviatoric strain for each number of cycles with $\alpha_{\sigma 0}$ = 0°, 22.5°, 45°,67.5° and 90° at CSR levels of 0.10, 0.15 and 0.20. Looking at the figure, the deviatoric strain slowly develops until the number of cycles reaches certain value, and then suddenly increases at onest of failure. It can be seen in the Fig. 8(a) that the case of $\alpha_{\sigma 0}$ = 0° was most prone to failure with the lowest resistance to the development of deviatoric strain, whereas the case of $\alpha_{\sigma 0}$ = 0° was the strongest in resisting the generation of deviatoric strain and had the least possibility of failure at CSR = 0.10. Similar observations are shown in Figs. 8(b) and 8(c) , where the deviatoric strain against the number of cycles for CSR = 0.15 and CSR = 0.20 are given, respectively.

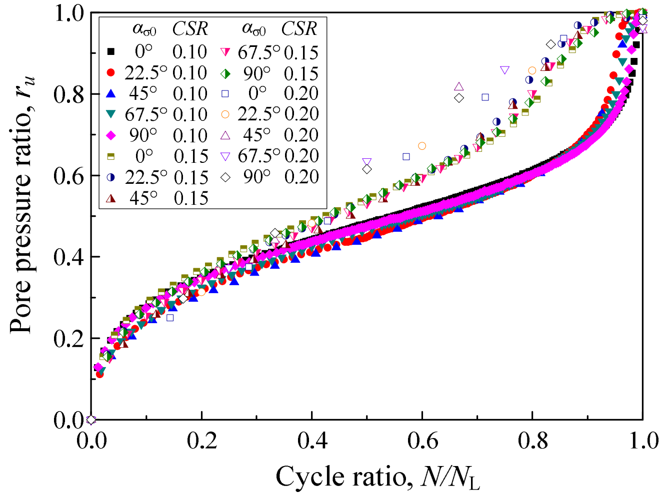

Fig.7 – Pore pressure ratio r_u as a function of normalized cycle number, N/N_L

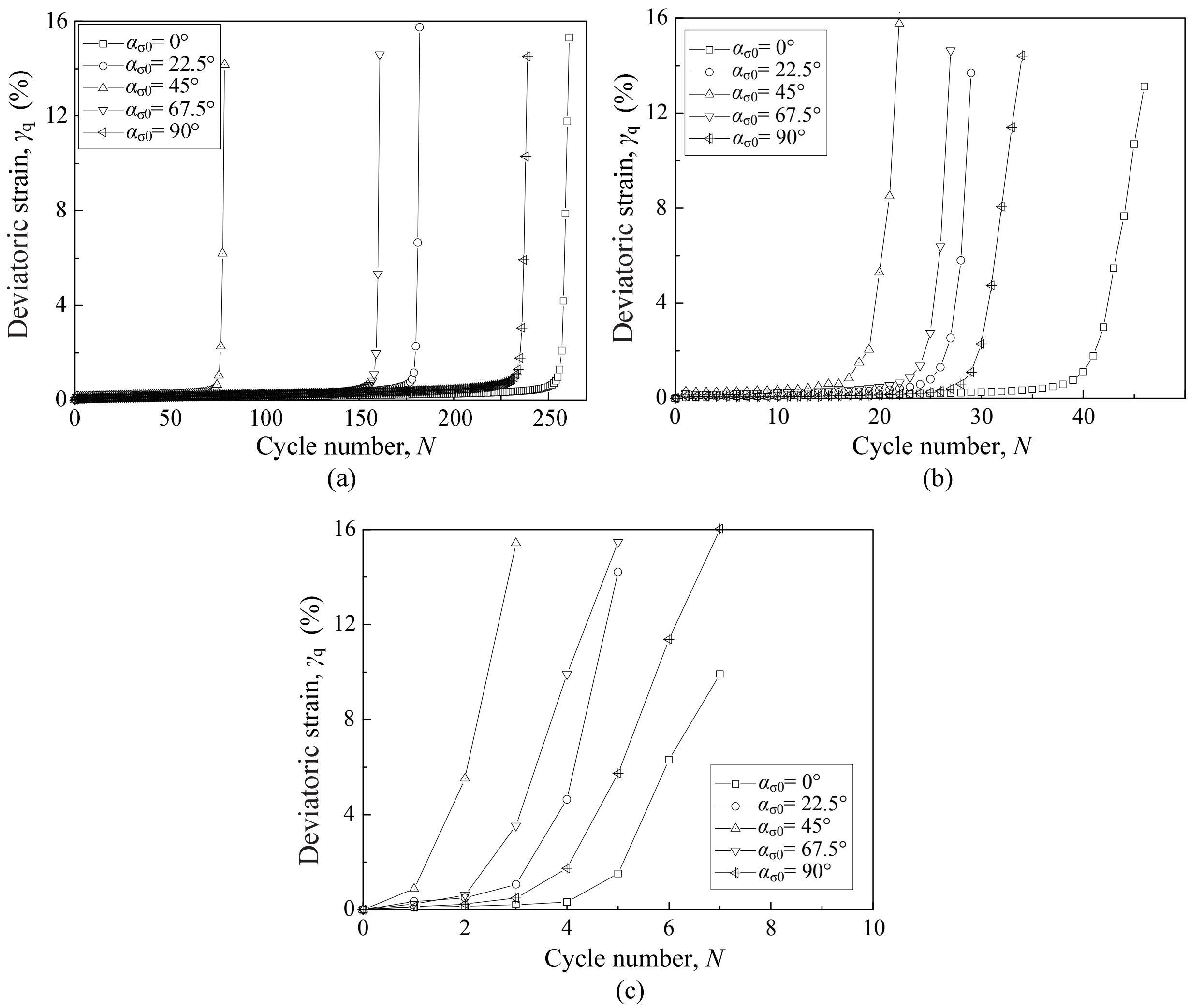

Fig. 8 – The relationship between initial loading direction $\alpha_{\sigma0}$, pore pressure ratio r_u, and the number of cycles N for the different cyclic stress ratio CSR: (a) CSR = 0.10; (b) CSR = 0.15; (c) CSR = 0.20

3.3 Effect of principal stress direction on cyclic shear strength

To characterise the cyclic shear strength for different $\alpha_{\sigma 0}$, the failure criterion needs to be defined. The failure for cyclic triaxial-torsional tests is usually defined as a deviatoric strain γ_q = 2.5% [16,17]. Fig. 9 shows the relationships between cyclic stress ratio and the number of cycles at various principal stress directions to induce 2.5% deviatoric strain. It is observed that the drastic differences in the number of cycles to failure clearly highlight the influence of principal stress direction. Increasing $\alpha_{\sigma 0}$ decreases the cyclic shear strength of silt up to a certain level, but the cyclic shear strength increases afterwards, which is consistent with the conclusion for dense sand obtained from Sato and Yoshida [7]. The main reason for this behaviour is that the stiffness of the specimen changes by initial loading direction due to the difference in the direction of cyclic loading. Therefore there is the effect of principal stress direction on the shear deformation behaviour during cyclic loading. The cyclic shear strength is determined by the principal stress direction at the initial time of cyclic loading and initial fabric anisotropy. The minimum strength occurs when the latent sliding surface is nearly parallel to the bedding plane. For medium dense silt in this study, the lowest cyclic shear strength is observed at $\alpha_{\sigma 0}$ = 45°. However, the minimum cyclic shear strength appears to occur when $\alpha_{\sigma 0}$ = 60° for dense sand obtained from Sato and Yoshida [7]. The significant difference in the $\alpha_{\sigma 0}$ value when the lowest cyclic shear strength turns up between two types of soils is possibly induced by their structure, particle shape and mineral ingredient.

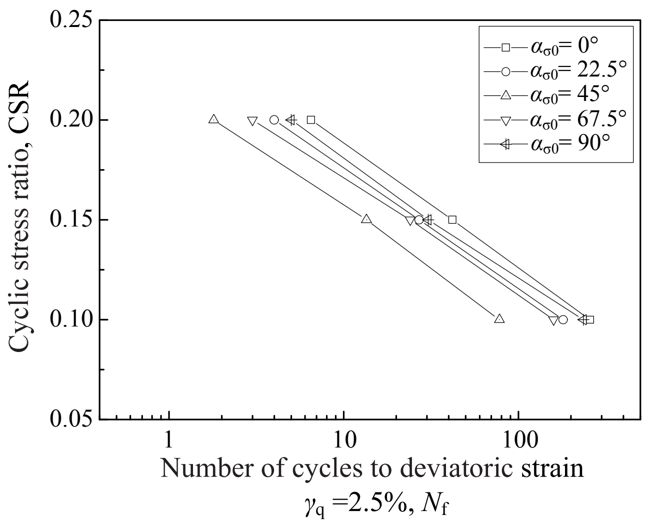

Fig. 9 – relations between the number of cycles to deviator strain γ_q = 2.5% and cyclic stress ratio

4. Conclusions

In this research, in order to investigate the effect of principal stress direction on the cyclic behaviour of saturated silt with a relative density of 50%, a series of undrained cyclic shear tests were conducted. The following conclusions were drawn from these tests:

(1) The principal stress direction has a significant effect on the behaviour of excess pore pressure and shear strain characteristics during undrained cyclic shear tests. Especially, the undrained cyclic shear behaviour is dependent on the initial principal stress direction of cyclic loading and initial fabric anisotropy of the specimen.

(2) The lowest cyclic shear strength is observed at the initial principal stress direction of cyclic loading $\alpha_{\sigma 0}$ = 45 °. This research indicates that strength anisotropy is determined by the principal stress direction of cyclic loading with respect to the bedding plane.

References

[1] Oda M (1972). Initial fabrics and their relations to mechanical properties of granular material. *Soils and foundations*, **12** (1), 17-36.

[2] Symes M, Gens A, Hight DW (1984). Undrained anisotropy and principal stress rotation in saturated sand. *Geotechnique*, **34** (1), 11-27.

[3] Yoshimine M, Ishihara K, Vargas W (1998). Effects of principal stress direction and intermediate principal stress on undrained shear behaviour of sand. *Soils and Foundations*, **38** (3), 179 -188.

[4] Sivathayalan S, Vaid YP (2002). Influence of generalized initial state and principal stress rotation on the undrained response of sands. *Canadian Geotechnical Journal*, **39** (1), 63-76.

[5] Luan Maotian, Xu Chengshun, He Yang, Guo Ying, Li Muguo (2006). Experimental study on the effect of orientation of principal stress on undrained behaviour of saturated loose sand under monotonic shearing. *Chinese Journal of Geotechnical Engineering*, **28** (9), 1085-1089 (in chinese).

[6] Kumruzzaman M, Yin JH (2010). Influences of principal stress direction and intermediate principal stress on the stress-strain-strength behaviour of completely decomposed granite. *Canadian Geotechnical Journal*, **47** (2), 164-179.

[7] Sato K, Yoshida N (1999). Effect of principal stress direction on undrained cyclic shear behaviour of dense sand.//*The Ninth International Offshore and Polar Engineering Conference*, International Society of Offshore and Polar Engineers.

[8] Sivathayalan S, Logeswaran P, Manmatharajan V (2015). Cyclic Resistance of a Loose Sand Subjected to Rotation of Principal Stresses[J]. *Journal of Geotechnical and Geoenvironmental Engineering*, **141** (3), 1024 -1039.

[9] Hight DW, Gens A, Symes MJ (1983). The development of a new hollow cylinder apparatus for investigating the effects of principal stress rotation in soils. *Geotechnique*, **33** (4), 355-383.

[10] Miura K, Miura S, Toki S (1986). Deformation behaviour of anisotropic dense sand under principal stress axes rotation. *Soils and Foundations*, **26** (1), 36-52.

[11] Tatsuoka F, Toki S, Miura S, Kato H, Okamoto M, Yamada S, Yasuda S, Tanizawa F (1986). Some factors affecting cyclic undrainedtriaxial strength of sand. *Soils and Foundations*, **26** (3), 99-116.

[12] Amini F, Chakravrty A (2004). LiquefactionTesting of layered sand-gravel composites. *Geotechnical Testing Journal*, **27** (1), 36-46.

[13] Cetin KO, Unutmaz B, Jeremic B (2012). Assessment of seismic soil liquefaction triggering beneath building foundation systems. *Soil Dynamics and Earthquake Engineering*, **43**, 160-173

[14] Seed HB, Martin PP, Lysmer J (1975). The generation and dissipation of pore water pressures during soil liquefaction. *Report No. EERC 75-26*, College of Engineering, University of California at Berkeley.

[15] Polito CP, Green RA, Lee J (2008). Pore pressure generation models for sands and silty soils subjected to cyclic loading. *Journal of Geotechnical and Geoenvironmental Engineering*, **134**(10), 1490-1500.

[16] Ishihara K, Yamazaki A (1984). Analysis of wave-induced liquefaction in seabed deposits of sand. *Soils and foundations*, **24** (3), 85-100.

[17] Huang B, Chen X, Zhao Y (2015). A new index for evaluating liquefaction resistance of soil under combined cyclic shear stresses. *Engineering Geology*, **199**, 125-139.